Molecular Vision 2002; 8:407-15 <http://www.molvis.org/molvis/v8/a48>
Received 24 September 2002 | Accepted 31 October 2002 | Published 31 October 2002

Mimecan/osteoglycin-deficient mice have collagen fibril abnormalities

Elena S. Tasheva,[1] Anja Koester,[2] Avelina Q. Paulsen,[1] Alexander S. Garrett,[1] Dan L. Boyle,[1] Harriet J. Davidson,[3] Min Song,[2] Niles Fox,[2] Gary W. Conrad[1]

[1]Division of Biology and [3]College of Veterinary Medicine, Kansas State University, Manhattan, KS; [2]Lilly Research Laboratories, Eli Lilly & Co., Indianapolis, IN

Purpose: To study the role of mimecan, a member of the small leucine-rich proteoglycans (SLRPs) gene family and one of the major components of the cornea and other connective tissues, mice that lack a functional mimecan gene were generated and characterized.
Methods: Mimecan-deficient mice were generated by gene-targeting using standard techniques. Mice were genotyped by Southern blot analysis. The absence of mimecan transcripts was confirmed by Northern blot analysis. Corneal clarity was examined by slit lamp biomicroscopy. The strength of the skin was evaluated using a biomechanical skin fragility test. Collagen morphology in cornea and skin preparations from mimecan-null and control wild-type mice was analyzed by transmission electron microscopy. The diameter of collagen fibrils in these tissues was determined by morphometric analysis.
Results: Mice lacking mimecan appear to develop normally, are viable and fertile. In a controlled laboratory environment they do not display an evident pathological phenotype compared to wild type mice. Examination of corneal clarity and measurements of corneal thickness show no significant changes in the cornea. However, a skin fragility test revealed a moderate reduction in the tensile strength of skin from mutant mice. Ultrastructural analyses show, on average, thicker collagen fibrils in both corneal and skin preparations from mimecan-null mice. Collagen fibrils from the cornea of mutant mice show an average diameter of 31.84±0.322 nm, versus 22.40±0.296 nm in their wild type litter-mates. The most pronounced increase in collagen fibril diameter was found in the skin of mimecan-null mice, who demonstrated an average diameter of 130.33±1.769 nm, versus 78.82±1.157 nm in the wild type mice. In addition, size variability and altered collagen morphology was detected in dorsal and tail skin preparations from the mutant mice.
Conclusions: The results of the present study demonstrate that mimecan, similar to other members of the SLRP gene family, has a role in regulating collagen fibrillogenesis in vivo. Further studies, such as functional challenges, an evaluation of potential compensation by other proteins (including members of the SLRP family), and generation of double-knockouts will be necessary to fully uncover physiological functions of mimecan in mice.

The extracellular matrix of connective tissues in the body of vertebrates contains a class of proteoglycans (PGs) known as small leucine-rich proteoglycans (SLRPs). These are encoded by separate genes and include 11 known members (reviewed in [1-3]). The SLRPs have core proteins ranging in size between 25 and 62 kDa and share a common protein structure; amino- and carboxy-terminal domains that are cysteine-rich and a central domain that is composed of 6 to 11 repeats of leucine-rich regions (LRRs). In addition, core proteins of SLRPs carry different glycosaminoglycan (GAG) side chains and/or have N-liked sugar modifications [4]. Several members of the SLRPs gene family have been shown to interact with other proteins, such as fibrilar collagens, growth factors, and growth factor receptors, and thus to influence extracellular matrix assembly, cellular growth and migration [1-3]. Direct binding to fibrilar collagens, mediated by the protein core, has been demonstrated for decorin, fibromodulin and lumican [5-8]. The GAG chains of SLRPs are believed to function in the maintenance of interfibrillar spacing and normal tissue hydration [1,4]. In the cornea, keratan sulfate GAGs appear to play an important role in the acquisition and maintenance of corneal transparency. This is illustrated by the absence, or altered glycosylation state, of corneal keratan sulfate-containing PGs in opaque corneal scars and in macular corneal dystrophy [9-12]. In vivo studies, using knock-out mice, where the expression of one or two SLRPs is deleted by gene targeting, provide further evidence that interactions between SLRPs and collagens are crucial for the assembly of the collagen network in connective tissues. For example, mice that lack lumican develop bilateral corneal haze, display skin laxity and delayed corneal epithelial wound healing. Mice that lack decorin have increased skin fragility, and mice that lack both biglycan and fibromodulin have gait impairment, ectopic ossification, and osteoarthritis, i.e. phenotypes consistent with dysfunctions of collagen networks [13-16].

Mimecan/osteoglycin, a member of the SLRPs gene family, was initially isolated in a truncated form from bovine bone and subsequently characterized as one of the three major keratan sulfate-containing PGs in the cornea, along with lumican and keratocan [17,18]. Encoded by a single copy gene

Correspondence to: Elena S. Tasheva, Division of Biology, Ackert Hall, Kansas State University, Manhattan, KS 66506-4901; Phone: (785) 532-6553; FAX: (785) 532-6653; email: est@ksu.edu

that is located on chromosome 9q22 in humans, mimecan is transcribed into at least 8 mRNAs, all of which are present in the cornea and all of which produce an identical protein that is conserved between mice, bovine and man, an indication of its functional importance [19-22]. A splice variant that changes the protein structure also has been desribed in birds [23]. Based on in vitro studies, mimecan may play a role in cellular growth control, as judged by ability of growth factors and cytokines to modulate its mRNA expression in corneal keratocytes and vascular smooth muscle cells [24,25]. This notion is further supported by the observation that the tumor suppressor protein p53 activates transcription of the bovine and human mimecan genes and that mimecan is absent in the majority of cancer cell lines and tumors [17,26,27]. As yet, there are no reports on how mimecan exerts its biological function.

To gain insight of the functional role of mimecan in vivo, we have generated mimecan-deficent mice. Here we report that the lack of mimecan leads to increase of collagen fibril diameter in the cornea and skin. These results demonstrate a role for mimecan in collagen fibrillogenesis.

METHODS

Construction of the targeting vector: A 12 kb *Sac* I genomic fragment containing the mouse mimecan gene was isolated from a λFix II (mouse 129/Sv genomic DNA library; Stratagene, La Jolla, CA) using a 900 bp cDNA fragment as a

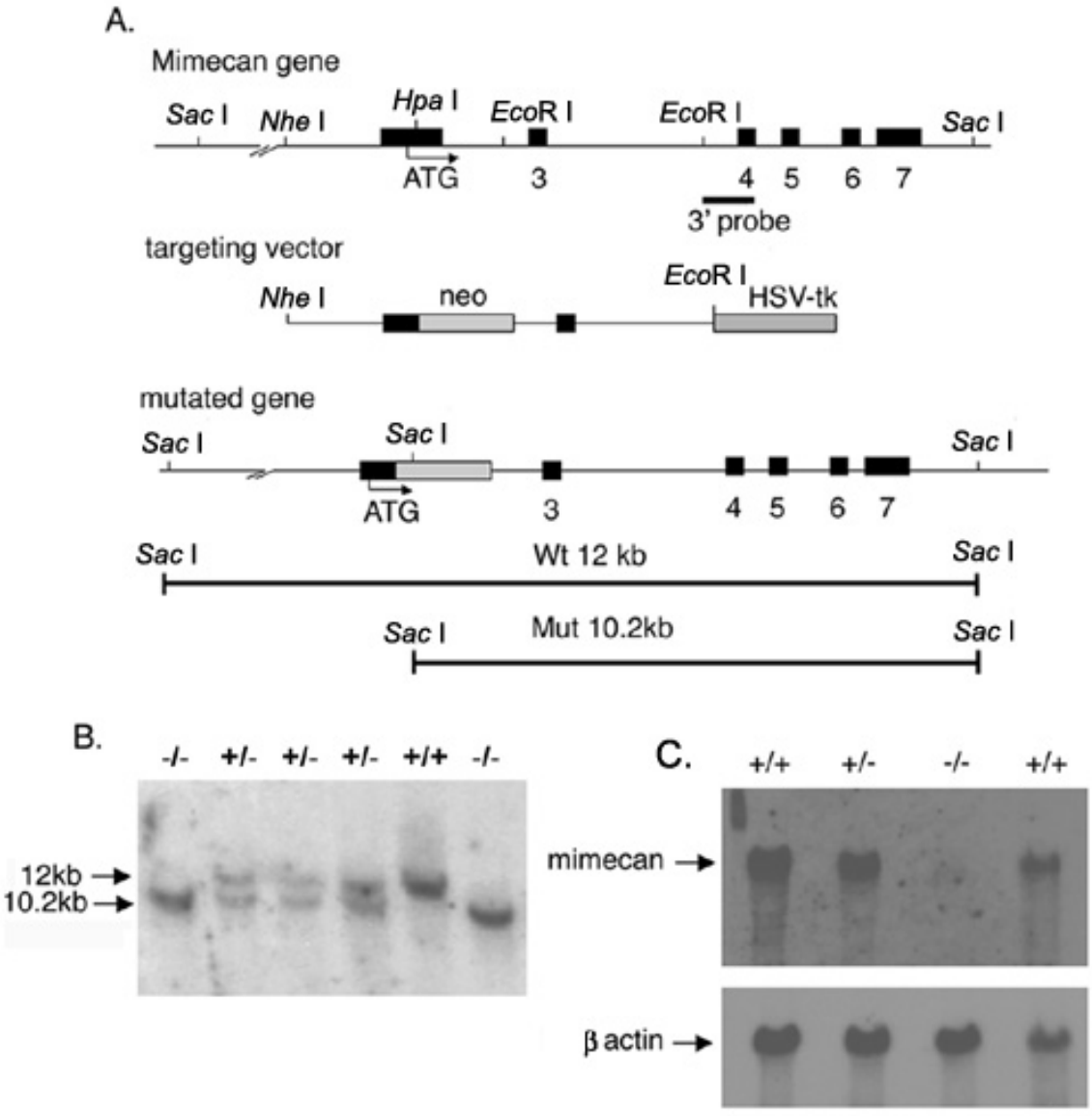

Figure 1. Mimecan gene targeting strategy and generation of mimecan-null mice. **A**: Structure of the mouse mimecan gene with the relevant restriction sites (top), the structure of the targeting vector (middle), and the structure of targeted gene (bottom). The wild-type allele (Wt) gives 12-kilobase pair (kb) DNA fragment, whereas the mutated allele gives 10.2 kb after digestion with *Sac* I. Exons are numbered and the translation initiation site (ATG) is indicated. **B**: Southern blot analysis of *Sac* I digested mouse genomic DNA isolated from wild-type (+/+), heterozygous (+/-) and mimecan-null (-/-) mice. **C**: Northern blot analysis of total RNA extracted from the lung of wild-type (+/+), heterozygous (+/-) or mimecan-null (-/-) mice that indicate an absence of mimecan mRNA in the mutant mice.

probe (Figure 1A). A pGTNN-tk backbone plasmid was used for construction of a mouse mimecan gene targeting vector. The plasmid pGTNN-tk, a derivative of pGT (gene targeting)-N29 (New England Biolabs Inc., Beverly, MA) cloning vector, contains the neomycin gene driven by the phosphoglycerate kinase (PGK) gene promoter and a herpes simplex virus thymidine kinase cassette (HSV-tk). A 2.5 kb genomic *Nhe* I/*Hpa* I fragment, containing the translation initiation sequence of the mouse mimecan gene, was subcloned into the *Avr* II site of pGTNN-tk vector. A 4.7 kb *Eco*R I fragment, containing part of intron 2, the entire exon 3 and a part of intron 3 of the mouse mimecan gene, was then cloned into the *Eco*R I site of pGTNN-tk vector. Thus, in the final gene targeting vector, the neo-resistance cassette interrupts the coding sequence in exon 2 after the His residue located in position 28 of the mouse mimecan gene (GenBank accession number D31951, Figure 1A).

Generation of mimecan-defficient mice: The linearized *Not* I targeting vector (25 μg) was used for transfection of $2x10^7$ E14 embryonic stem cells (ES cells, derived from 129/O1a mice) as described [28]. After selection with G418 and gancyclovir for 8, days 288 resistant and independent ES cell clones were isolated and analyzed for homologous recombination by Southern blotting. To check for additional random integration events the positive clones were also hybridized with an internal neomycin-specific probe. Three positive clones were identified and used for microinjection into C57BL/6 blastocysts. Male chimeric founders were mated to C57BL/6 females and agouti-coated offspring were analyzed for germ line transmission of the mimecan mutation by Southern blot analysis. Littermates of these offsspring were used for all studies.

All experiments were performed in compliance with the ARVO statement for use of animals in ophthalmic and vision research. Mice were housed in the animal care facility of KSU according to NIH guidelines (NIH publication No. 86-23,1985) and IACUC approved protocols.

Southern and Northern blot analyses: Genomic DNA was isolated from mouse tail biopsies as described [29]. A DNA fragment spanning the 3'-region of intron 3 and 5'-region of exon 4 of the mouse mimecan gene (Figure 1A, 3'-probe) was used as a probe for Southern blot analysis to identify correctly targeted ES cells and to confirm the mouse genotype (Figure 1B). Targeted disruption of the mimecan gene introduces an additional *Sac* I recognition site and consequently the probe detects a 12 kb *Sac* I fragment with the wild type allele and a 10.2 kb *Sac* I fragment with the correctly targeted mutant allele. Southern blot analysis was performed as described [30].

Total RNA was isolated from mouse lung using guanidine isothiocyanate and Northern blotting was performed as described [30]. Mimecan mRNA was detected using a 900 bp mouse mimecan cDNA probe. The same blot was stripped and re-hybridized with a βactin probe (Figure 1D). The βactin probe was purchased from Clontech Laboratories, Inc., Palo Alto, CA.

Histopathology and clinical pathology: Six 1-year-old mimecan-null mice and their control litter-mates were used for histopathological analysis. The following tissues were fixed and stained with hematoxylin and eosin, and examined microscopically; adrenals, bone marrow/sternum, brain, colon, duodenum, eye/hardarian gland, heart, ileum, jejunum, kidney, knee joint, liver, lung, lymph node, ovary/uterus, pancreas, pituitary, preputial gland, prostate, salivary gland, sciatic nerve, seminal vesicle, skeletal muscle, skin, mammary gland, spinal cord, spleen, stomach, testis, thymus, thyroid, trachea/esophagus, ear, and tail.

Blood samples were collected from homozygous and heterozygous mice, and their control litter-mates (n=6). The following clinical chemistry and hematological parameters were measured; total protein, albumin, globulin, cholesterol, triglycerides, total bilirubin, creatinin, glucose, alkaline phosphatase, alanine aminotransferase, aspratate aminotransferase, blood urea nitrogen, hemoglobin, white and red blood cells counts, MCV, MCH, and differential white blood cell counts.

X-Ray examination of bones was performed at the KSU Veterinary Medical Teaching Hospital on two wild-type and two mimecan-null mice (8 months old) anesthesized with methofluorane.

Slit-Lamp examination of eyes: A vertical slit-lamp biomicroscope (Nikon, Nippon Kogaku K.K., Japan) with attached

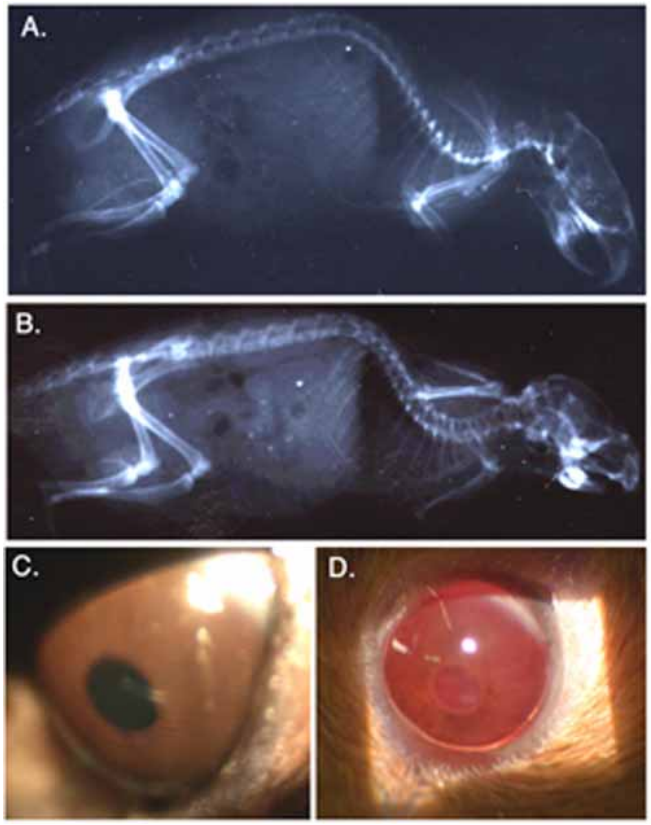

Figure 2. X-ray examination of wild type and mimecan-null mouse bones. X-ray examination of bones of wild type mouse (**A**) and mimecan-null mouse (**B**) shows no major bone abnormalities in the mutant mice. A full view of eye examinations for corneal clarity of age-matched wild type mouse (**C**) and mimecan-null mouse (**D**) did not reveal changes in corneal clarity in the mutant mouse.

digital camera (Nikon E995) was used to examine and photograph eyes of mimecan-null and wild-type mice.

Skin tension test: Skin samples were prepared from the dorsal skin of age-matched mimecan-null mice and their wild-type litter-mates. A dumbbell-shaped plastic template was used to obtain skin samples (4 cm x 2 cm whose midpoint contained a region cut to 1.0 cm width). These were kept moist with saline. Thickness measurements were taken with a micrometer.

The tension test was performed using a Warner-Bratzler Meat Shear to generate constant torque (G-R Manufacturing, Manhattan, KS), with force measured with a Dillon digital basic force gauge (Dillon/Quality Plus, Inc., Kansas City, MO). The tensile skin strength was determined as the maximal load at rupture (in grams) of sample in the narrow central region (1.0 cm width).

Transmission electron microscopy and image analysis: The corneas and small portions of skin and tail from mimecan-null and wild type mice of the same age were fixed in 2% paraformaldehyde, 2% glutaraldehyde, and 0.1 M PIPES (pH 7.3) for 3 h on ice. The speciments were postfixed in PIPES-buffered 1% osmium tetroxide, dehydrated in graded ethanol, followed by graded acetone, infiltrated and embedded in Spurr epoxy resin as described [31]. Thin sections were stained with 2% uranyl acetate and Reynold's lead citrate, examined with a transmission electron microscope (Philips CM100) and regions containing cross-sections of collagen fibrils were photographed at 80 kV for image analysis. Five micrographs from

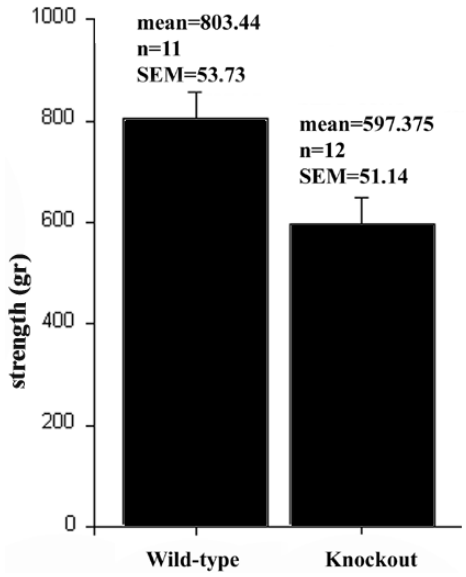

Figure 3. Skin tensile strength measurements. The force required to break 1.0 cm width strips of skin prepared from each knock-out and control mouse was determined as follows: Whole skin was immobilized on a flat surface under uniform tension. Six cuts required to produce 3 identical, parallel strips of skin of 1.0 cm width were made simultaneously with a 6 bladed cutting device (designed by R. Lundquist), with skin flattened beneath a slotted plastic mask. From each mouse, two strips were used. Force required to break each strip was determined as described in methods. The means were compared using the one way ANOVA-F-test. This test produced a p value of 0.0113323. At an α of 0.025 there is sufficient evidence to indicate significant differences between the mean value of mimecan-null versus the mean value of wild-type mice.

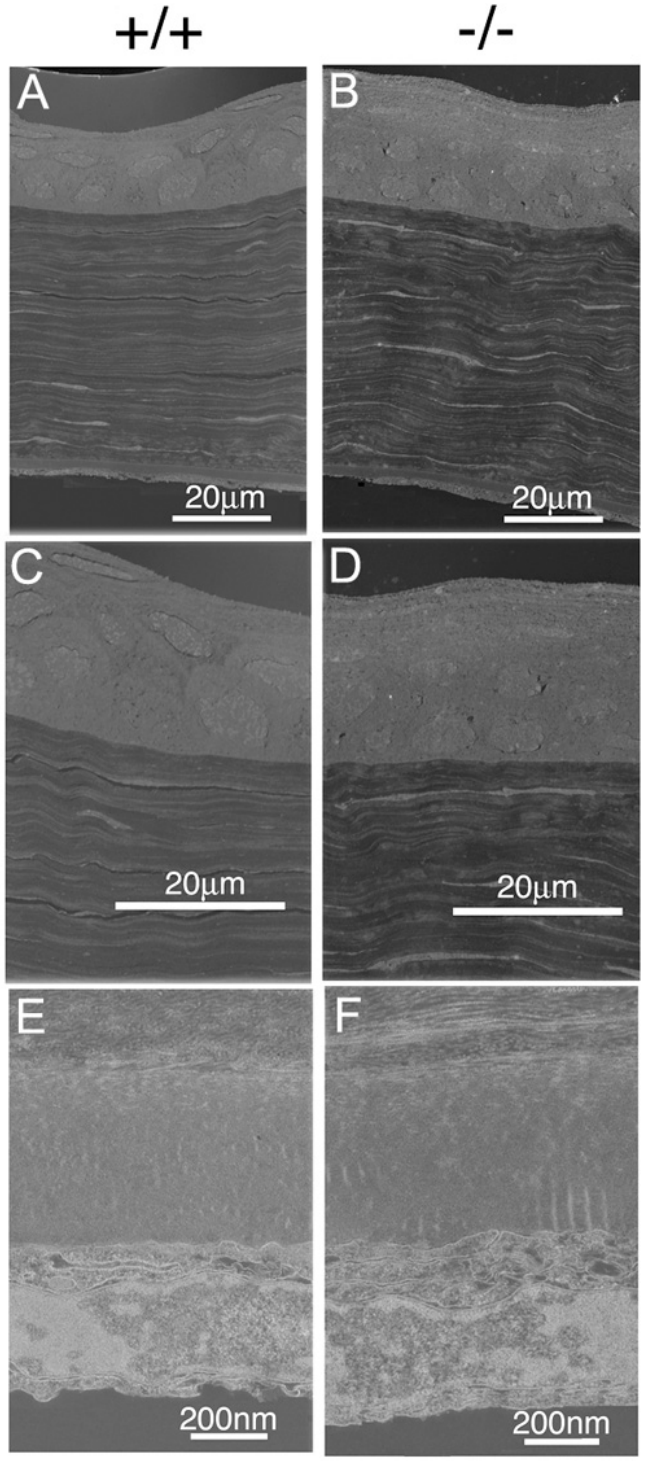

Figure 4. TEM of corneas. Transmission electron micrographs of corneas from wild type (+/+) and mimecan-null mice (-/-). **A** and **B**: Longitudinal sections of the cornea; **C** and **D**: Higher magnification of the epithelial sublayer of the cornea; **E** and **F**: Descemet's and endothelial layers of the cornea. No significant differences in the cornea and corneal layers can be noted.

transverse sections of each corneal stroma, dorsal and tail skin were digitized on a flatbed scanner at a resolution of 600 dpi. Each sample was assigned a random number, the diameter of 631 to 940 collagen fibrils were measured manually and results presented in a histogram.

RESULTS

Generation of mimecan-null mice: The mimecan gene was targeted with a vector containing 7.2 kb of DNA sequence interrupted in the second exon with a neomycin resistance cassette (Figure 1A). Neomycin resistance was used for positive selection, whereas the thymidine kinase cassette, cloned 3' of the targeting construct, was used as a negative selection marker. Homologous recombination was detected by Southern blotting of *Sac* I-digested genomic DNA using a 3' external probe (Figure 1A). Three independent clones were identified and used to produce male chimeric founders. These were mated to C57BL/6 females to generate an inbred strain. Crosses of heterozygous mice resulted in the generation of mice that were homozygous for the mutant mimecan gene. The mice were genotyped by Southern blotting (Figure 1B). To confirm that mice homozygous for the targeted mutation do not express mimecan, Northern blots were probed with mouse mimecan cDNA probe. Mimecan mRNA could not be detected in tissues extracts of mimecan-null mice whereas under the same hybridization conditions mimecan mRNA was clearly detected in tissue extracts from wild-type mice (Figure 1C).

Clinical pathology and histopathology of mimecan-null mice: Mimecan-null mice appeared to develop normally, were viable and grew to normal size. Clinical chemistry and hematological profile, performed on three 6-month-old mice, revealed no significant difference in parameters (see methods) in samples from mimecan-deficient and wild-type mice. X-ray examination was performed to determine whether the lack of mimecan could cause bone abnormalities. No significant defects in bone structure of mimecan-null mice were detected (Figure 2A and Figure 2B). Slit-lamp examination was performed to assess potential role of mimecan in regulating corneal transparency. Fifteen mimecan-null mice, between ages of 2 months to 1 year and 2 months, were examined. No significant changes in corneal clarity were detected in mimecan-null mice that were not also seen in wild-type mice (Figure 2C and Figure 2D). Follow-up eye exams over 6-8 months did not reveal significant changes in corneal clarity in mimecan-null mice. Light microscopic investigations of all tissues listed in methods also were performed. Similarly, no major anatomical and histopathological defects in mimecan-null mice that were not also seen in wild-type mice were detected.

Since reduced tensile strength of the skin has been reported in mice that lack two other SLRPs, decorin and lumican [13,15], the tensile strength of skin samples isolated from

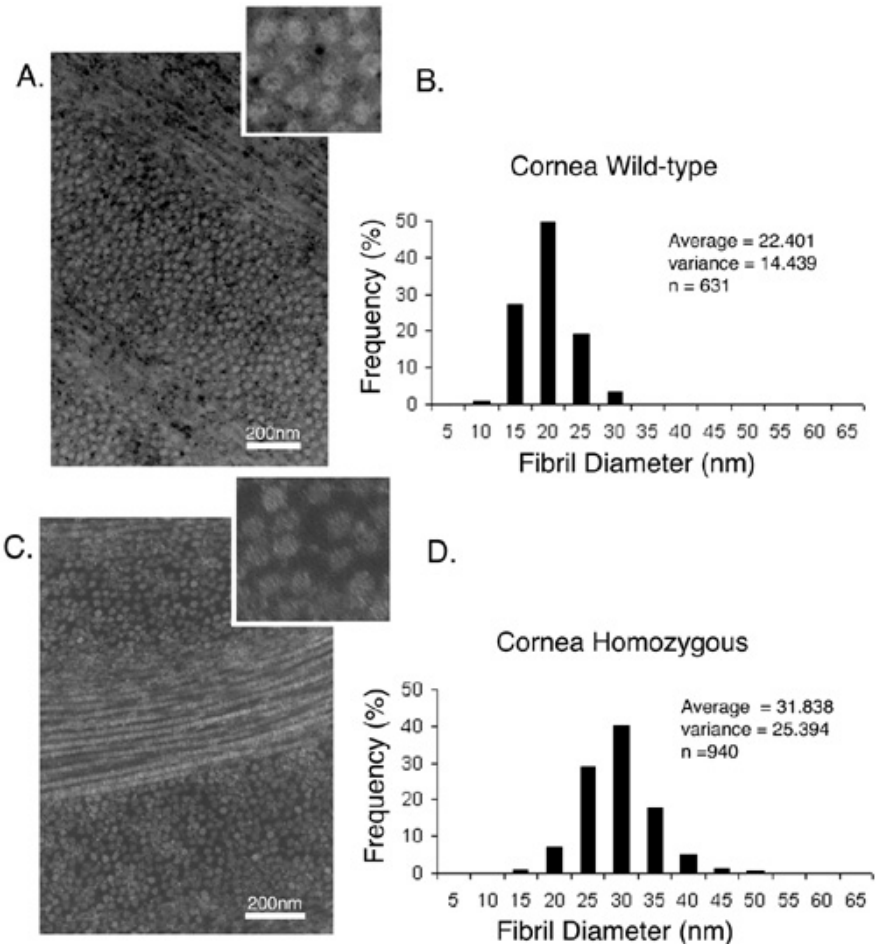

Figure 5. TEM of collagen fibrils from mouse corneal stroma. Transmission electron micrographs containing cross-sections of collagen fibrils from corneal stroma from wild-type (**A**) and mutant (**C**) mice. Morphometric analysis of corneal collagen fibrils in wild-type (**B**) and in mutant (**D**) mice. Fibril diameter was measured as described in methods and presented in a histogram. The average fibril diameter, the variance and the total number (n) of fibrils measured are indicated.

mimecan-deficient mice was similarly measured. Skin samples from five 1-year-old mimecan-null and their age-matched wild-type mice were used for this study. One dorsal and two lateral skin speciments per animal having an identical dumbbell-shape were obtained. The samples were gripped into a custom made tensile testing machine and stretched to rupture with a constant strain rate of 1 mm/s. Tensile strength was calculated from maximal load at rupture (in grams) of sample in the narrow central region (in cm). The results from this study are presented in Figure 3. The skin from mimecan-null mice ruptured at approximately 475 g, whereas the skin from wild-type mice ruptured at approximately 741 g. These data demonstrated that mimecan-null mice exhibit moderate reduction in the tensile strength of the skin. Significant changes in the thickness of the skin from mutant mice were not detected.

Electron microscopy analysis of cornea from mimecan-null mice: Transmission electron microscopy was used for more detailed analysis of the cornea and corneal collagen architecture. As shown in Figure 4A and Figure 4B, general organization of the cornea from mimecan-null mice appeared similar to that of wild-type mice. Low magnification micrographs obtained from five 1-year-old animals were used to determine the thickness of corneal layers. The thickness of epithelial, stromal and Descemet's layer in the cornea from

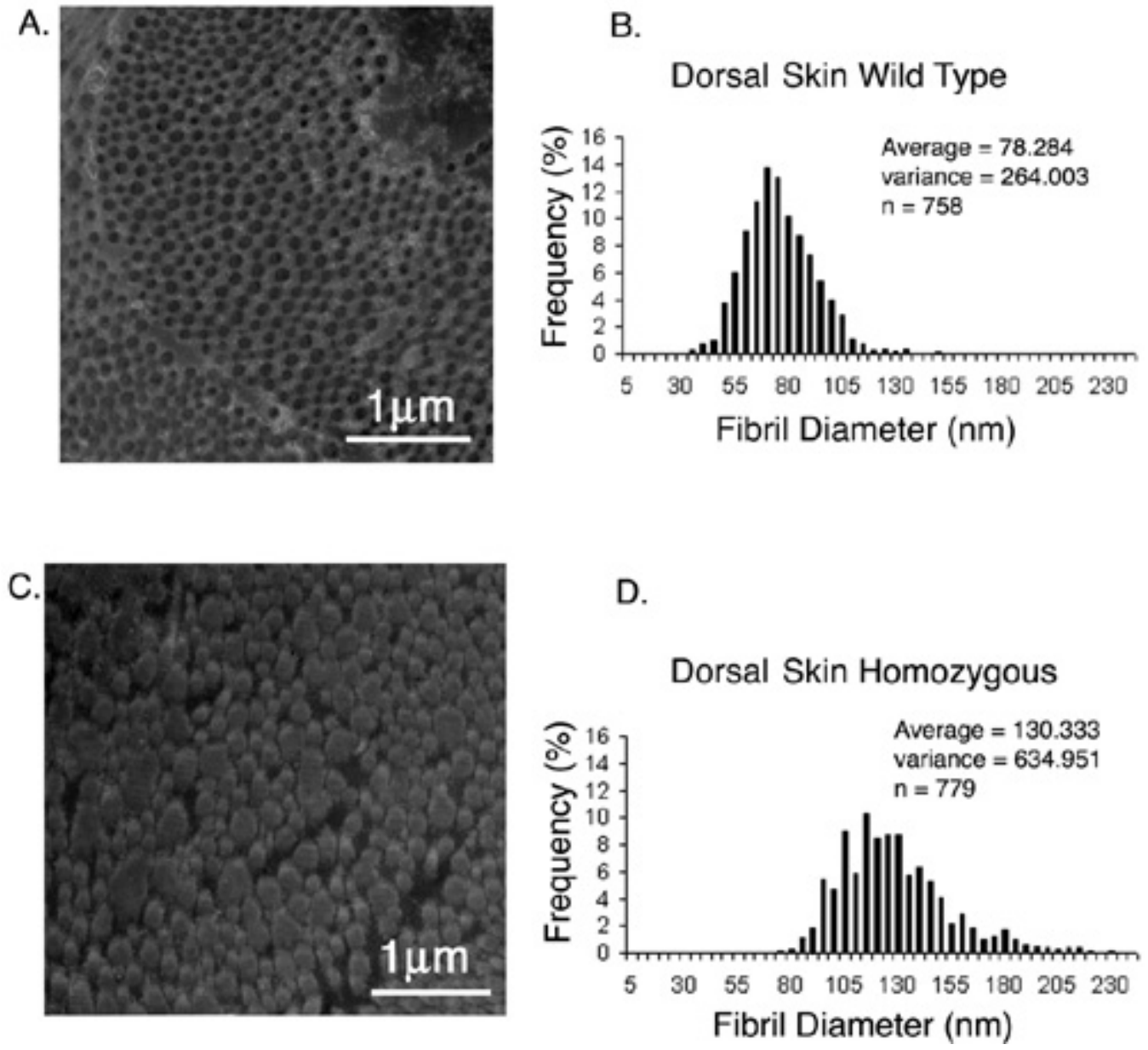

Figure 6. TEM of collagen fibrils from mouse dorsal skin. Transmission electron micrographs containing cross sections of collagen fibrils from dorsal skin of wild type mouse (**A**) and mimecan-null mouse (**C**). Morphometric analysis of skin collagen fibrils (**B** and **D**). Notice the significantly larger diameter of collagen fibrils in mimecan-null mice (**D**).

mutant mice was comparable to the thickness of these layers in the wild-type mice (Figure 4, compare Figure 4C with Figure 4D and Figure 4E with Figure 4F). The structure of collagen fibrils in the corneal stroma was additionally analyzed. As shown in Figure 5, corneal collagen fibrils morphology appeared similar in both corneas. However, it could be noted that in mimecan-null mice collagen fibrils appeared more loosely packed compared to the closely packed fibrils in wild-type mice (Figure 5, compare Figure 5A with Figure 5C). Collagen fibril diameters distribution was determined for both corneas. An increase in average fibril diameter in mimecan-null mice; 31.84±0.322 nm, versus 22.40±0.296 nm in the wild type mice, was detected. In addition, the distribution of fibril diameters showed a slight shift toward larger diameters, up to over 50 nm in mimecan-null mice (Figure 5, compare Figure 5B with Figure 5D).

Abnormal collagen fibril morphology in the skin of mimecan-null mice: Electron microscopic analysis of dorsal and tail skin dermis samples clearly showed abnormalities in the structure of collagen fibrils. In dorsal skin samples from mimecan-null mice collagen fibrils were less orderly packed, appeared thicker than in wild-type mice, and some fibrils exhibited irregular shape in cross-sections (Figure 6, compare Figure 6A with Figure 6C). Morphometric analysis demonstrated a significant increase in the average fibril diameter in mutant mice; 130.33±1.769 nm, versus 78.82±1.157 nm in the wild type mice (Figure 6, compare Figure 6B with Figure 6D). Electron micrographs from tail skin dermis showed an even greater variability in size and shape of collagen fibrils in samples from mutant mice when compared to these from wild-type mice (Figure 7, compare Figure 7A and Figure 7B with Figure 7D and Figure 7E). Morphometric analysis showed that the average collagen fibril diameter was only slightly larger in mimecan-null mice (Figure 7F) compared to that of wild-type mice (Figure 7C); 92.48 nm versus 80.64 nm respectively. However, in skin samples from mutant mice, a wider range in fibril diameter between 35 and 200 nm was noted. In contrast, wild-type tail skin showed relatively uniform collagen fibril diameters, ranging between 35 and 135 nm (Figure 7C and Figure 7F).

DISCUSSION

In the present study we have generated mimecan-deficient mice and analyzed their phenotypic changes. Inactivation of the mimecan gene resulted in a rather subtle phenotype, mice were viable and fertile, and did not show major anatomical

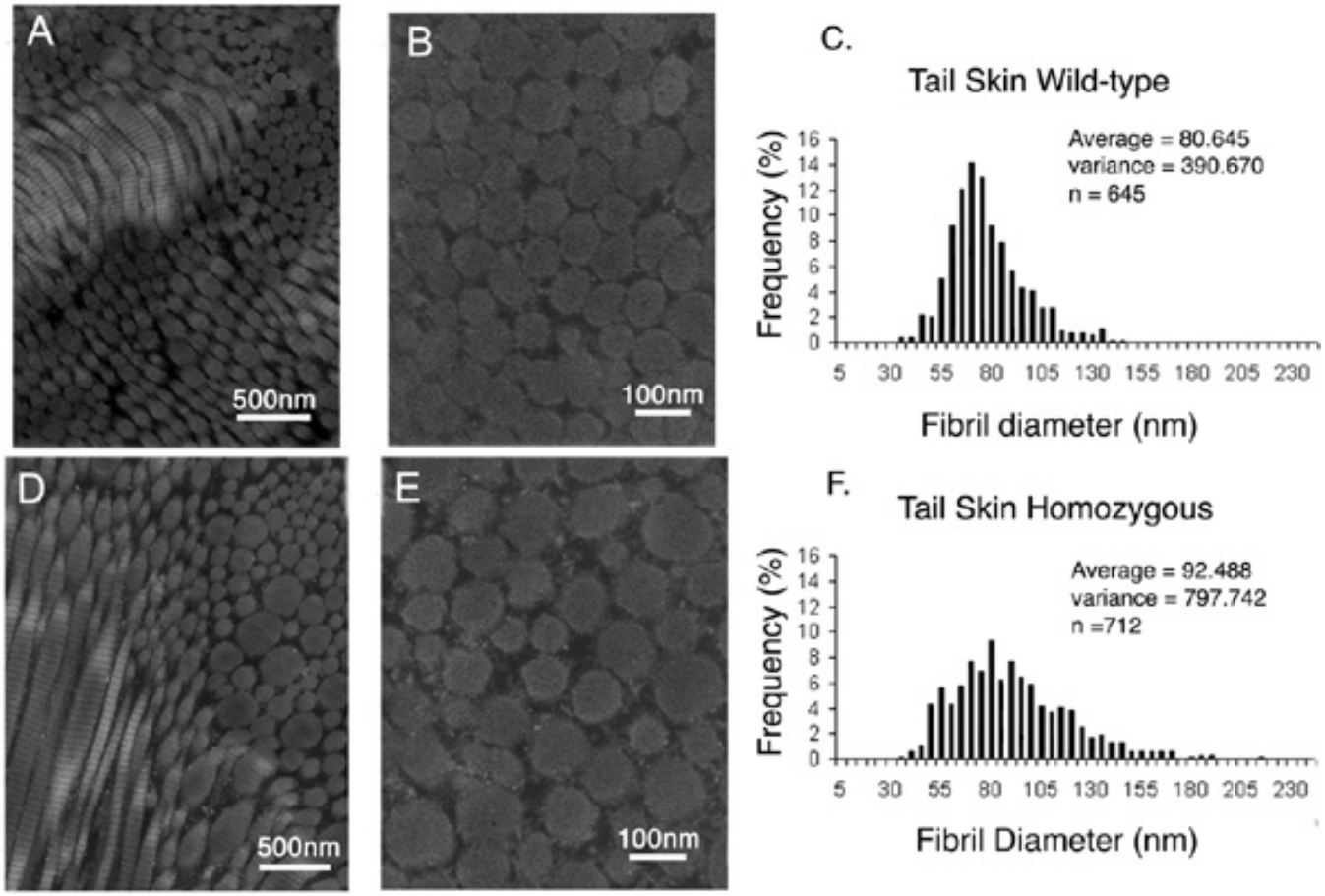

Figure 7. TEM of collagen fibrils from mouse tail skin. Transmission electron micrographs containing cross sections of collagen fibrils from tail skin of wild type mouse (**A** and **B**) and mimecan-null mouse (**D** and **E**). Morphometric analysis of tail skin fibrils (**C** and **F**). Notice that the range of distribution is larger in mimecan-null mice (**F**).

and histological defects. Considering the existence of other members of the SLRP gene family that could compensate for the lack of mimecan, the observed phenotype was not entirely surprising. Furthermore, knock-outs for other SLRP members, such as fibromodulin, similarly show subtle phenotypic changes [32].

Corneal development in the mimecan-null mice appeared normal and changes in corneal clarity were not detected. Significant changes in the thickness of corneal epithelial, stromal and Descemet's layers also were not detected. Ultrastructural analysis, however, revealed that in mutant mice corneal collagen fibrils were thicker and relatively loosely packed compared to the wild-type mice. These results indicate a role for mimecan in corneal collagen fibrillogenesis. It is of interest to note that, to date, an evident corneal phenotype has been described only in lumican-deficient mice [13]. Mice deficient for other SLRPs have normal corneal collagen architecture. The absence of clinically detectable changes in corneal thickness and/or clarity in these mice may be explained by the requirement for keratan sulfate for corneal transparency. In decorin-null mice, for example, the overall corneal keratan sulfate levels were not affected, since decorin carries a choindroitin sulfate GAG chain. Chondroitin/dermatan sulfate GAG chains seem to play a minor role in corneal transparency, as judged by the in vivo observations that the decorin-null mice have normal corneal collagen [15]. Mimecan has been reported to carry keratan sulfate GAG chains in bovine and human corneas, but its core protein appears to lack this modification in mice [18]. Thus, the results presented in this report are in agreement with previous observations and provide additional evidence for the importance of keratan sulfate for corneal transparency. They demonstrate that mimecan plays a role in the regulation of corneal collagen fibril diameter and interfibrillar spacing, although not a major one in mice. A major role could be predicted for bovine and human species, where mimecan, along with lumican and keratocan, are corneal keratan sulfate-carrying PGs.

Compared to lumican- and decorin-null mice, skin fragility in our mice was relatively moderate. However, the structure of collagen fibrils in dorsal and tail skin samples is clearly altered as evidenced by transmission electron microscopy. The main changes appeared similar to those described in mice that lack other SLRP members, i.e. the presence of thicker and irregularly shaped fibrils and non-uniform interfibrillar spacing, results that demonstrate a major role for mimecan in regulating the collagen fibrollogenesis in skin.

Collagen fibrillogensis is known as a complex process, and many factors influence fibril growth, diameter and interfibrillar spacing. These include the genes for fibrilar collagens, enzymes processing the nascent collagens, fibril-associated proteins, and collagen-binding proteoglycans. Mutations of several types of collagen genes, such as type III procollagen, collagen α1(I) and α2(I) have been described as leading causative factors of the human syndrome, designated Ehlers-Danlos syndrome (EDS). Mutations in enzymes processing nascent collagen fibrils also can cause EDS [33,34]. Considering the phenotypic changes in mice that lack SLRP genes reported so far, together with the results presented in this study, one might expect that mutations of collagen-binding SLRP genes will be detected in some patients that will fall into separate EDS groups.

ACKNOWLEDGEMENTS

This work was supported by NIH Grants EY13395 to GWC and EST and EY00952 to GWC. We thank R.Lundquist, G-R Manufacturing, for use of the meat shear and force gauge and for design and fabrication of the 6-bladed cutting device.

REFERENCES

1. Iozzo RV. The family of the small leucine-rich proteoglycans: key regulators of matrix assembly and cellular growth. Crit Rev Biochem Mol Biol 1997; 32:141-74.
2. Iozzo RV. The biology of the small leucine-rich proteoglycans. Functional network of interactive proteins. J Biol Chem 1999; 274:18843-6.
3. Svensson L, Oldberg A, Heinegard D. Collagen binding proteins. Osteoarthritis Cartilage 2001; 9:S23-8.
4. Prydz K, Dalen KT. Synthesis and sorting of proteoglycans. J Cell Sci 2000; 113:193-205.
5. Rada JA, Cornuet PK, Hassell JR. Regulation of corneal collagen fibrillogenesis in vitro by corneal proteoglycan (lumican and decorin) core proteins. Exp Eye Res 1993; 56:635-48.
6. Svensson L, Narlid I, Oldberg A. Fibromodulin and lumican bind to the same region on collagen type I fibrils. FEBS Lett 2000; 470:178-82.
7. Svensson L, Heinegard D, Oldberg A. Decorin-binding sites for collagen type I are mainly located in leucine-rich repeats 4-5. J Biol Chem 1995; 270:20712-6.
8. Kresse H, Liszio C, Schonherr E, Fisher LW. Critical role of glutamate in a central leucine-rich repeat of decorin for interaction with type I collagen. J Biol Chem 1997; 272:18404-10.
9. Hassell JR, Newsome DA, Krachmer JH, Rodrigues MM. Macular corneal dystrophy: failure to synthesize a mature keratan sulfate proteoglycan. Proc Natl Acad Sci U S A 1980; 77:3705-9.
10. Hassell JR, Cintron C, Kublin C, Newsome DA. Proteoglycan changes during restoration of transparency in corneal scars. Arch Biochem Biophys 1983; 222:362-9.
11. Funderburgh JL, Cintron C, Covington HI, Conrad GW. Immunoanalysis of keratan sulfate proteoglycan from corneal scars. Invest Ophthalmol Vis Sci 1988; 29:1116-24.
12. Plaas AH, West LA, Thonar EJ, Karcioglu ZA, Smith CJ, Klintworth GK, Hascall VC. Altered fine structures of corneal and skeletal keratan sulfate and chondroitin/dermatan sulfate in macular corneal dystrophy. J Biol Chem 2001; 276:39788-96.
13. Chakravarti S, Magnuson T, Lass JH, Jepsen KJ, LaMantia C, Carroll H. Lumican regulates collagen fibril assembly: skin fragility and corneal opacity in the absence of lumican. J Cell Biol 1998; 141:1277-86.
14. Saika S, Shiraishi A, Liu CY, Funderburgh JL, Kao CW, Converse RL, Kao WW. Role of lumican in the corneal epithelium during wound healing. J Biol Chem 2000; 275:2607-12.
15. Danielson KG, Baribault H, Holmes DF, Graham H, Kadler KE, Iozzo RV. Targeted disruption of decorin leads to abnormal collagen fibril morphology and skin fragility. J Cell Biol 1997; 136:729-43.

16. Ameye L, Aria D, Jepsen K, Oldberg A, Xu T, Young MF. Abnormal collagen fibrils in tendons of biglycan/fibromodulin-deficient mice lead to gait impairment, ectopic ossification, and osteoarthritis. FASEB J 2002; 16:673-80.
17. Madisen L, Neubauer M, Plowman G, Rosen D, Segarini P, Dasch J, Thompson A, Ziman J, Bentz H, Purchio AF. Molecular cloning of a novel bone-forming compound: osteoinductive factor. DNA Cell Biol 1990; 9:303-9.
18. Funderburgh JL, Corpuz LM, Roth MR, Funderburgh ML, Tasheva ES, Conrad GW. Mimecan, the 25-kDa corneal keratan sulfate proteoglycan, is a product of the gene producing osteoglycin. J Biol Chem 1997; 272:28089-95.
19. Ujita M, Shinomura T, Kimata K. Molecular cloning of the mouse osteoglycin-encoding gene. Gene 1995; 158:237-40.
20. Tasheva ES, Funderburgh ML, McReynolds J, Funderburgh JL, Conrad GW. The bovine mimecan gene. Molecular cloning and characterization of two major RNA transcripts generated by alternative use of two splice acceptor sites in the third exon. J Biol Chem 1999; 274:18693-701.
21. Tasheva ES, Corpuz LM, Funderburgh JL, Conrad GW. Differential splicing and alternative polyadenylation generate multiple mimecan mRNA transcripts. J Biol Chem 1997; 272:32551-6.
22. Tasheva ES, Pettenati M, Von Kap-Her C, Conrad GW. Assignment of mimecan gene (OGN) to human chromosome band 9q22 by in situ hybridization. Cytogenet Cell Genet 2000; 88:326-7.
23. Dunlevy JR, Beales MP, Berryhill BL, Cornuet PK, Hassell JR. Expression of the keratan sulfate proteoglycans lumican, keratocan and osteoglycin/mimecan during chick corneal development. Exp Eye Res 2000; 70:349-62.
24. Long CJ, Roth MR, Tasheva ES, Funderburgh M, Smit R, Conrad GW, Funderburgh JL. Fibroblast growth factor-2 promotes keratan sulfate proteoglycan expression by keratocytes in vitro. J Biol Chem 2000; 275:13918-23.
25. Shanahan CM, Cary NR, Osbourn JK, Weissberg PL. Identification of osteoglycin as a component of the vascular matrix. Differential expression by vascular smooth muscle cells during neointima formation and in atherosclerotic plaques. Arterioscler Thromb Vasc Biol 1997; 17:2437-47.
26. Tasheva ES, Maki CG, Conrad AH, Conrad GW. Transcriptional activation of bovine mimecan by p53 through an intronic DNA-binding site. Biochim Biophys Acta 2001; 1517:333-8.
27. Tasheva ES. Analysis of the promoter region of human mimecan gene. Biochim Biophys Acta 2002; 1575:123-9.
28. Koster A, Montkowski A, Schulz S, Stube EM, Knaudt K, Jenck F, Moreau JL, Nothacker HP, Civelli O, Reinscheid RK. Targeted disruption of the orphanin FQ/nociceptin gene increases stress susceptibility and impairs stress adaptation in mice. Proc Natl Acad Sci U S A 1999; 96:10444-9.
29. Laird PW, Zijderveld A, Linders K, Rudnicki MA, Jaenisch R, Berns A. Simplified mammalian DNA isolation procedure. Nucleic Acids Res 1991; 19:4293.
30. Fox N, Song M, Schrementi J, Sharp JD, White DL, Snyder DW, Hartley LW, Carlson DG, Bach NJ, Dillard RD, Draheim SE, Bobbitt JL, Fisher L, Mihelich ED. Transgenic model for the discovery of novel human secretory non-pancreatic phospholipase A2 inhibitors. Eur J Pharmacol 1996; 308:195-203.
31. Spooner BS, Paulsen A. Basal lamina anionic sites in the embryonic submandibular salivary gland: resolution and distribution using ruthenium red and polyethyleneimine as cationic probes. Eur J Cell Biol 1986; 41:230-7.
32. Svensson L, Aszodi A, Reinholt FP, Fassler R, Heinegard D, Oldberg A. Fibromodulin-null mice have abnormal collagen fibrils, tissue organization, and altered lumican deposition in tendon. J Biol Chem 1999; 274:9636-47.
33. Byers PH. Ehlers-Danlos syndrome: recent advances and current understanding of the clinical and genetic heterogeneity. J Invest Dermatol 1994; 103:47.
34. Pope FM, Burrows NP. Ehlers-Danlos syndrome has varied molecular mechanisms. J Med Genet 1997; 34:400-10.

The print version of this article was created on 31 Oct 2002. This reflects all typographical corrections and errata to the article through that date. Details of any changes may be found in the online version of the article.